Synthesis, structure and optical limiting properties of organoruthenium–chalcogenide clusters

ARTICLE *in* JOURNAL OF ORGANOMETALLIC CHEMISTRY · MARCH 2005

Impact Factor: 2.17 · DOI: 10.1016/j.jorganchem.2004.12.018

8 AUTHORS, INCLUDING:

Mark G Humphrey
Australian National University
336 PUBLICATIONS **6,443** CITATIONS

SEE PROFILE

Marek Samoc
Wroclaw University of Technology
384 PUBLICATIONS **6,238** CITATIONS

SEE PROFILE

Available online at www.sciencedirect.com
SCIENCE DIRECT®
Journal of Organometallic Chemistry 690 (2005) 1487–1497
Journal of Organometallic Chemistry
www.elsevier.com/locate/jorganchem

Synthesis, structure and optical limiting properties of organoruthenium–chalcogenide clusters

Mark G. Humphrey [a,*], Bryce Lockhart-Gillett [b], Marek Samoc [c], Brian W. Skelton [d], Vicki-Anne Tolhurst [b,*], Allan H. White [d], Adele J. Wilson [b], Brian F. Yates [b]

[a] Department of Chemistry, Australian National University, Canberra, ACT, 0200, Australia
[b] School of Chemistry, University of Tasmania, Private Bag 75, Hobart, TAS, 7001, Australia
[c] Laser Physics Centre, Research School of Physical Sciences and Engineering, Australian National University, Canberra, ACT, 0200, Australia
[d] Chemistry M313, University of Western Australia, Crawley, WA 6009, Australia

Received 10 November 2004; accepted 14 December 2004

Abstract

Treatment of $Ru_3(CO)_{12}$ with Ph_3PS affords the compounds $[Ru_3(\mu_3\text{-}S)_2(CO)_{9-n}(PPh_3)_n]$ ($n = 1$ (**1a**), 2 (**2a**)) and $[Ru_3(\mu_3\text{-}S)(\mu_3\text{-}CO)(CO)_7(PPh_3)_2]$ (**3a**) as the major products. Single crystal X-ray diffraction studies of $[Ru_3(\mu_3\text{-}S)_2(CO)_8(PPh_3)]$ and $[Ru_3(\mu_3\text{-}S)(\mu_3\text{-}CO)(CO)_7(PPh_3)_2]$ show these two classes of compounds to contain square pyramidal Ru_3S_2 and trigonal pyramidal Ru_3S metal cores, respectively, with the latter being isostructural to the analogous selenide cluster compound. The clusters $[Ru_3(\mu_3\text{-}E)_2(CO)_{9-n}(PPh_3)_n]$ (E = S, $n = 1$; E = Se, $n = 2$) readily undergo ligand displacement reactions with PPh_3 to afford the compounds $[Ru_3(\mu_3\text{-}E)_2(CO)_6(PPh_3)_3]$ (E = S, **5a**; E = Se **5b**). The mixed chalcogenide cluster, $[Ru_3(\mu_3\text{-}S)(\mu_3\text{-}Se)(CO)_7(PPh_3)_2]$ (**6**), was prepared from the reaction of $[Ru_3(\mu_3\text{-}S)(\mu_3\text{-}CO)(CO)_7(PPh_3)_2]$ and $SePPh_3$. The optical limiting properties of the complexes **1a,b, 2a,b, 5a,b** have been measured by the *Z*-scan technique employing 40 ns pulses at 523 nm; power limiting was observed for all clusters under our experimental conditions.

Keywords: Chalcogenide; Ruthenium; Cluster; X-ray structure; Optical power limiting

1. Introduction

Topical interest centres on the isolation of metal chalcogenide clusters as well-defined molecular precursors to quantum devices for applications in materials science and surface chemistry due to their unique photoelectric and catalytic properties [1]. Nonlinear optical properties have been reported for a number of inorganic metal chalcogenide clusters with varying core geometries [2–5]. A common feature of these cluster compounds is the μ_3-bridging binding mode of the chalcogenide which provides stability to the cluster toward light-induced fragmentation caused by the electronic transition between the skeletal bonding- and anti-bonding orbitals.

The oxidative transfer of chalcogen atoms to zero-valent metal compounds is a well-established method for the preparation of metal chalcogenide cluster compounds. A number of organoiron and ruthenium selenide clusters containing phosphine ligands have been prepared from the reaction of $[M_3(CO)_{12}]$ (M = Fe, Ru) with phosphine selenide reagents [6–10]. Other organoiron and ruthenium chalcogenide clusters have been prepared from zero-valent metal compounds using reagents such as alkyl sulfides [11], H_2S [12], diphenyl diselenide [13], and $[Cp^{\#}{}_2Nb(Te_2H)]$ ($Cp^{\#} = C_5Me_5$ or C_5Me_4Et) [14].

* Corresponding authors. Tel.: +61 3 62262169; fax: +61 3 62262858.
E-mail address: vickianne.tolhurst@utas.edu.au (V.-A. Tolhurst).

0022-328X/$ - see front matter © 2005 Elsevier B.V. All rights reserved.
doi:10.1016/j.jorganchem.2004.12.018

In order to identify correlations in optical limiting properties with structural and composition features of organometallo chalcogenide clusters, we have prepared a number of organoruthenium sulfide clusters by treating $[Ru_3(CO)_{12}]$ with Ph_3PS. The clusters obtained are similar to those from the analogous reaction using Ph_3PSe. We have also prepared the mixed chalcogenide cluster, $[Ru_3(\mu_3\text{-}S)(\mu_3\text{-}Se)(CO)_7(PPh_3)_2]$, from the chalcogenide insertion reaction between $[Ru_3(\mu_3\text{-}S)(\mu_3\text{-}CO)(CO)_7(PPh_3)_2]$ and $SePPh_3$. The trisubstituted PPh_3 clusters were also prepared using ligand displacement reactions. This enabled the effect of ligand substitution and chalcogenide substitution on the optical limiting activity of the compounds to be investigated.

2. Results and discussion

2.1. Synthesis and characterisation

Treatment of $Ru_3(CO)_{12}$ with excess Ph_3PS (8 equiv.) in the presence of Me_3NO leads to the formation of the 50 electron clusters $[Ru_3(\mu_3\text{-}S)_2(CO)_8(PPh_3)]$ (**1a**), $[Ru_3(\mu_3\text{-}S)_2(CO)_7(PPh_3)_2]$ (**2a**) and the 48 electron cluster $[Ru_3(\mu_3\text{-}S)(\mu_3\text{-}CO)(CO)_7(PPh_3)_2]$ (**3a**) as major products. The compounds were characterised by IR and ^1H, $^{13}C\{^1H\}$ and $^{31}P\{^1H\}$ NMR spectroscopies, and microanalysis. The ν(CO) stretches of clusters **1a** and **2a** confirmed that all carbonyl ligands were terminally bound to the ruthenium centres, while the presence of a ν(CO) stretch at 1664 cm^{-1} in the spectrum of **3a** confirmed the presence of a μ_3-capping carbonyl ligand with the other ligands all being terminally bound. The products are similar to those prepared from the analogous reaction of $Ru_3(CO)_{12}$ with Ph_3PSe [8,10], but the reaction appears to be much slower as multiple products are still obtained in the time taken to selectively afford the thermodynamically favoured cluster $[Ru_3(\mu_3\text{-}Se)_2(CO)_7(PPh_3)_2]$ (**2b**). The product distribution for both reactions appears to be highly dependent on the concentration of the reaction; we found that if smaller amounts of solvent were used in the reactions, $[Ru_3(\mu_3\text{-}E)_2(CO)_7(PPh_3)_2]$ could be the only product isolated.

The $^{31}P\{^1H\}$ NMR spectra of the sulfide cluster compounds are similar to the spectra of their analogous selenium clusters. In general, the resonances for the sulfur clusters appear slightly downfield compared to those of the selenide clusters due to the greater electronegativity of sulfur. The $^{31}P\{^1H\}$ NMR spectrum of $[Ru_3(\mu_3\text{-}S)_2(CO)_8(PPh_3)]$ (**1a**) exhibits a single resonance at 62.6 ppm, indicative of one species in solution. The $^{31}P\{^1H\}$ NMR spectrum of $[Ru_3(\mu_3\text{-}S)_2(CO)_7(PPh_3)_2]$ (**2a**) exhibits four resonances: two sharp singlets at 60.2 and 45.5 ppm and two broader resonances at 56.3 and 39.9 ppm. This resonance pattern is similar to that of the analogous selenide cluster, **2b** [15], and is indicative of two species being present. Previous analysis of the spectrum of **2b** assigned the broader resonances to the species where the two PPh_3 ligands occupy non-equivalent positions on the two basal ruthenium metals as seen in the solid state, and the other two sharp resonances are due to the isomer where the two PPh_3 ligands are coordinated to two linked ruthenium metals, although the existence of this isomer for PPh_3 has not been confirmed [15].

In order to add validity to the possibility that the second isomer observed in the $^{31}P\{^1H\}$ NMR spectra of **2a** and **2b** exists as a result of ligand migration, we undertook a theoretical investigation using Density Functional Theory (DFT) to calculate the relative energies of the two possible isomers. The optimised structures of the $[Ru_3(\mu_3\text{-}E)_2(CO)_7(PMe_3)_2]$ (E = S (**4a**), Se (**4b**)) isomers were initially based on the solid-state structure of $[Ru_3(\mu_3\text{-}Se)_2(CO)_7(PPh_3)_2]$ [15] but were allowed to optimise without constraint using the B3LYP level of theory. The PPh_3 ligands were replaced by PMe_3 in the calculated structures for computational feasibility. Isomer **A** of both **4a** and **4b** is analogous to that observed in the solid-state structure of $[Ru_3(\mu_3\text{-}Se)_2(CO)_7(PPh_3)_2]$ and has one PMe_3 ligand occupying a pseudo-equatorial position on one basal ruthenium with the other PMe_3 ligand occupying a pseudo-axial position on the other basal ruthenium (Fig. 1(a)). Isomer **B** of both **4a** and **4b** also has one PMe_3 ligand occupying a pseudo-equatorial position on one of the basal ruthenium atoms but the second PMe_3 ligand is now coordinated to the apical ruthenium (Fig. 1. (B)). The calculations show that isomer B for both **4a** and **4b** is only slightly higher in energy than isomer **A** with the energy difference between the two isomers being 8.9 and 9.1 kJ mol^{-1} for **4a** and **4b**, respectively, indicating that both isomers could easily exist in solution at room temperature.

Occasionally the cluster compound $[Ru_3(\mu_3\text{-}S)_2(CO)_6(PPh_3)_3]$ (**5a**) was observed as a minor product from the reaction outlined in Scheme 1. Similarly, $[Ru_3(\mu_3\text{-}Se)_2(CO)_6(PPh_3)_3]$ (**5b**) has also been observed in the product distribution for the analogous reaction using $SePPh_3$ [10]. These compounds can readily be prepared from the ligand displacement reaction of the Ru_3E_2 clusters where the CO ligands can be substituted by additional phosphine ligands. The trisubstituted cluster $[Ru_3(\mu_3\text{-}S)_2(CO)_6(PPh_3)_3]$ (**5a**) can be prepared from the reaction of $[Ru_3(\mu_3\text{-}S)_2(CO)_8(PPh_3)]$ (**2a**) with two equivalents of PPh_3, in the presence of Me_3NO (Scheme 2). The initial formation of $[Ru_3(\mu_3\text{-}S)_2(CO)_7(PPh_3)_2]$ in the reaction indicates that the ligand substitution is a stepwise reaction, as expected. The trisubstituted cluster $[Ru_3(\mu_3\text{-}Se)_2(CO)_6(PPh_3)_3]$ (**5b**) can also be prepared from the ligand substitution reaction between $[Ru_3(\mu_3\text{-}Se)_2(CO)_7(PPh_3)_2]$ (**2b**) and PPh_3. The IR spectra of the two clusters indicate that all carbonyl ligands are

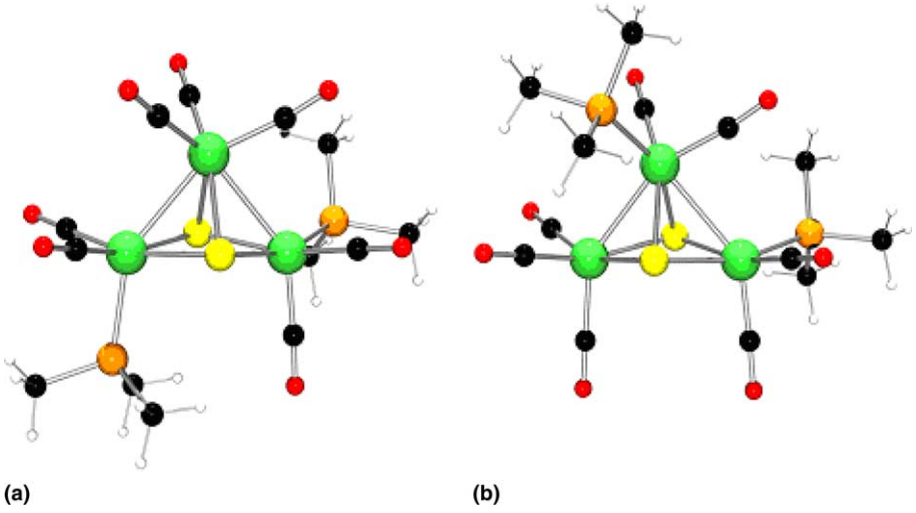

Fig. 1. Optimised geometries for the isomers of $[Ru_3(\mu_3\text{-}E)_2(CO)_7(PMe_3)_2]$ (E = S (**4a**), Se (**4b**)).

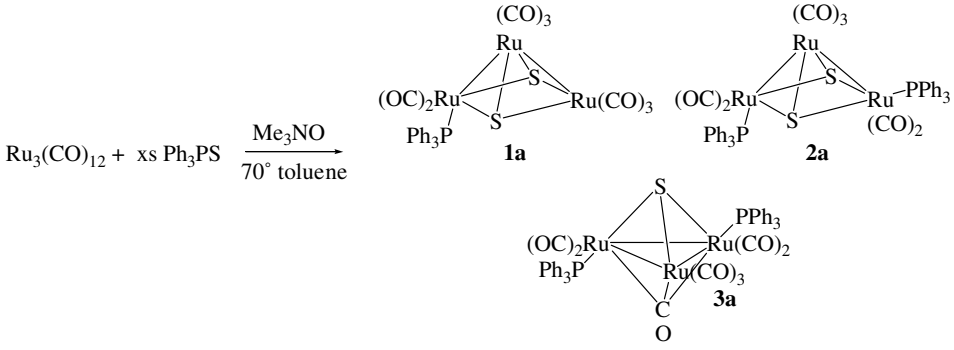

Scheme 1. Preparation of ruthenium sulfide clusters **1a**, **2a** and **3a.**

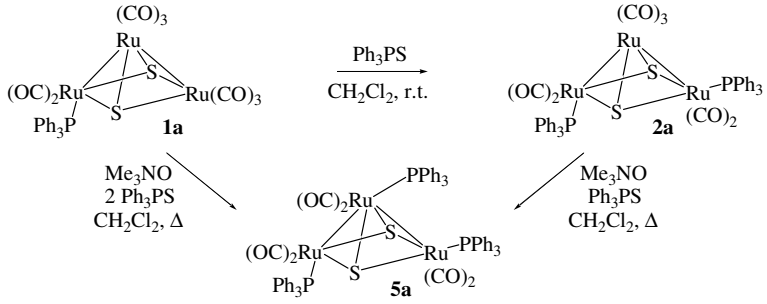

Scheme 2. Ligand substitution of $[Ru_3(\mu_3\text{-}S)_2(CO)_{(9-n)}(PPh_3)_n]$ (n = 1, 2).

terminally bound. The $^{31}P\{^1H\}$ NMR spectra of the two clusters show similar features. The $^{31}P\{^1H\}$ NMR spectrum of **5b** contains a sharp resonance at 48.3 ppm and a very broad resonance at 46.1 ppm integrating as 1:2, indicating that the three PPh_3 ligands are in two different environments, i.e. one bound to the apical ruthenium and two bound to the two basal ruthenium atoms. The $^{31}P\{^1H\}$ NMR spectrum of **5a** only contains one sharp resonance at 48.2 ppm but it may be possible that the broad resonance seen in the spectrum of **5b** is indistinguishable from the baseline in the spectrum of **5a**; the temperature dependence of this signal was not pursued.

Previous studies by Predieri and co-workers [10] have indicated the presence of $[Ru_3(\mu_3\text{-}Se)(\mu_3\text{-}CO)(CO)_7(PPh_3)_2]$ (**3b**) in the product distribution from the chalcogen insertion reaction of $[Ru_3(CO)_{12}]$ and Ph_3PSe to be due to its role as an intermediate to the formation of $[Ru_3(\mu_3\text{-}Se)_2(CO)_7(PPh_3)_2]$, confirmed by the isolation of $[Ru_3(\mu_3\text{-}Se)_2(CO)_7(PPh_3)_2]$ from the reaction of

$[Ru_3(\mu_3\text{-Se})(\mu_3\text{-CO})(CO)_7(PPh_3)_2]$ with Ph_3PSe. This led us to use this approach to prepare mixed chalcogenide organoruthenium cluster compounds. The reaction of $[Ru_3(\mu_3\text{-S})(\mu_3\text{-CO})(CO)_7(PPh_3)_2]$ (**3a**) with Ph_3PSe in the presence of Me_3NO afforded the mixed chalcogenide cluster $[Ru_3(\mu_3\text{-S})(\mu_3\text{-Se})(CO)_7(PPh_3)_2]$ (**6**). This reaction was chosen, rather than using $[Ru_3(\mu_3\text{-Se})(\mu_3\text{-CO})(CO)_7(PPh_3)_2]$ (**3b**) and Ph_3PS, because of the weaker P═Se bond, as reflected in the difference in reaction times in the formation of $[Ru_3(\mu_3\text{-S})_2(CO)_7(PPh_3)_2]$ and $[Ru_3(\mu_3\text{-Se})_2(CO)_7(PPh_3)_2]$ as mentioned previously. The IR spectrum of **6** indicates that all carbonyl ligands are terminally bound as in the homochalcogenide cluster compounds. The $^{31}P\{^1H\}$ NMR spectrum of **6** also exhibits a similar resonance pattern to the homochalcogenide clusters, $[Ru_3(\mu_3\text{-E})_2(CO)_7(PPh_3)_2]$, consisting of two sharp resonances at 58.1 and 54.4 ppm and two broad resonances at 55.1 and 44.7 ppm, consistent with two species in solution. A second product was also isolated from the reaction which we have not been able to fully characterise. This has been initially identified as $[Ru_3(\mu_3\text{-Se})_2(CO)_6(PPh_3)_3]$, based on infrared and ^{31}P NMR data, suggesting that ligand redistribution may also occur during these types of reactions (see Scheme 3).

2.2. Solid-state structures of $[Ru_3(\mu_3\text{-S})_2(CO)_8(PPh_3)]$ (**1a**) and $[Ru_3(\mu_3\text{-E})(\mu_3\text{-CO})(CO)_7(PPh_3)_2]$ (E = S (**3a**), Se (**3b**))

The cluster $[Ru_3(\mu_3\text{-S})_2(CO)_8(PPh_3)]$ (**1a**) crystallises from the slow evaporation of a $CHCl_3$ solution as orange block crystals in the monoclinic space group *C*2/*c*. Table 1 lists selected crystallographic data and bond distances and angles are listed in Table 2. The compound crystallises with one cluster molecule in the asymmetric unit along with 1.5 $CHCl_3$ solvent molecules, both components disordered (Fig. 2). The cluster core comprises three ruthenium centres and two μ_3-capping sulfur atoms giving the core an overall distorted square pyramid geometry with a Ru_2S_2 basal plane, similar to that of the selenide cluster $[Ru_3(\mu_3\text{-Se})_2$-

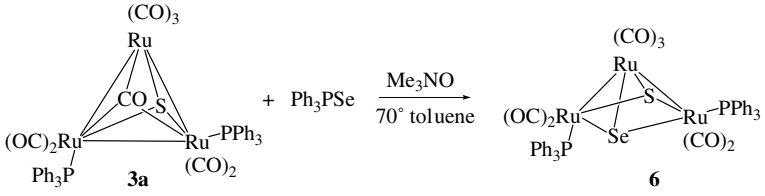

Scheme 3. Preparation of mixed chalcogenide cluster **6**.

Table 1
Selected crystallographic data for the compounds $[Ru_3(\mu_3\text{-S})_2(CO)_8(PPh_3)] \cdot 3/2CHCl_3$ (**1a**), $[Ru_3(\mu_3\text{-E})(\mu_3\text{-CO})(CO)_7(PPh_3)_2] \cdot CH_2CL_2$ (E = S (**3a**), Se (**3b**))

Complex	**1a**	**3a**	**3b**
Formula	$C_{27.5}H_{16.5}Cl_{4.5}O_8PRu_3S_2$	$C_{45}H_{32}Cl_2O_8P_2Ru_3S$	$C_{45}H_{32}Cl_2O_8P_2Ru_3Se$
M	1032.8	1168.8	1215.8
Crystal system	Monoclinic	Triclinic	Triclinic
Space group	*C*2/c	$P\bar{1}$	$P\bar{1}$
a (Å)	25.327(2)	10.667(5)	10.559(1)
b (Å)	10.2787(7)	11.6187(13)	11.371(1)
c (Å)	28.339(2)	20.242(6)	20.280(2)
α (°)	90	88.941(15)	89.308(2)
β (°)	105.086(2)	87.21(4)	87.221(2)
γ (°)	90	66.44(2)	66.770(2)
U (Å^3)	7123.2(9)	2296.7(12)	2234.8(4)
D_c (g cm^{-3})	1.926	1.690	1.807
Z	8	2	2
μ (mm^{-1})	1.8	1.252	2.06
$T_{min/max}$	0.79	0.80	0.80
$2\theta_{max}$ (°)	75	50	58
N_t	70899	8317	20837
$N(R_{int})$	18697 (0.038)	8066 (0.0235)	10869 (0.039)
N_o ($F > 4\sigma(F)$)	15137	7024[a]	7959
R	0.040	0.025	0.044
R_w	0.083	0.062	0.051
GoF	1.12	1.061	1.14
T (K)	150	298	150

[a] $I_o > 2\sigma(I)$.

Table 2
Selected bond distances and angles for $[Ru_3(\mu_3\text{-}S)_2(CO)_8(PPh_3)] \cdot 3/2CHCl_3$ (E = S) (**1a**)

Bond distances (Å)			
Ru(1)–Ru(3)	2.8121(3)	Ru(2)–Ru(3)	2.7362(4)
Ru(2)–E(1)	2.3900(7)	Ru(1)–E(1)	2.3755(7)
Ru(1)–E(2)	2.3711(7)	Ru(3)–E(1)	2.4021(7)
Ru(3)–E(2)	2.4199(7)	Ru(2)–E(2)	2.3798(7)
Ru(1)–P(1)	2.2988(8)		
Bond angles (°)			
Ru(2)–Ru(3)–Ru(1)	82.257(11)	Ru(1)–E(2)–Ru(2)	100.39(2)
Ru(3)–Ru(1)–E(1)	54.382(19)	Ru(1)–E(2)–Ru(3)	71.89(2)
Ru(3)–Ru(2)–E(1)	55.39(2)	Ru(2)–E(2)–Ru(3)	69.50(2)
Ru(1)–Ru(3)–E(1)	53.505(17)	Ru(3)–Ru(1)–E(2)	54.868(19)
Ru(2)–Ru(3)–E(1)	54.97(2)	Ru(3)–Ru(2)–E(2)	55.94(2)
Ru(1)–E(1)–Ru(2)	99.97(2)	Ru(1)–Ru(3)–E(2)	53.257(19)
Ru(1)–E(1)–Ru(3)	72.11(2)	Ru(2)–Ru(3)–E(2)	54.559(18)
Ru(2)–E(1)–Ru(3)	69.64(2)	P(1)–Ru(1)–E(1)	101.09(3)
E(1)–Ru(1)–E(2)	79.13(2)	P(1)–Ru(1)–E(2)	106.07(3)
E(1)–Ru(2)–E(2)	78.66(2)	P(1)–Ru(1)–Ru(3)	148.83(2)
E(1)–Ru(3)–E(2)	77.65(2)		

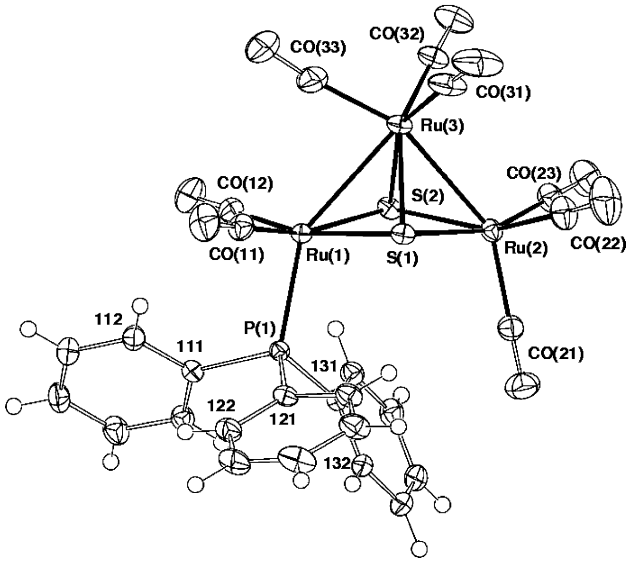

Fig. 2. Molecular projection of $[Ru_3(\mu_3\text{-}S)_2(CO)_8(PPh_3)]$ (**1a**) projected through the Ru_2S_2 plane.

$(CO)_7(PPh_3)_2]$ [15]. In cluster **1a**, the PPh_3 substituent is bound to Ru(1) in a pseudo-axial position. This differs from the Fe/Se analogue [16] in which the triphenylphosphine group is pseudo-equatorial to the basal plane.

The lengths of the two Ru–Ru bonds (2.8121(3), 2.7362(4) Å) differ by approximately 0.08 Å, the longer bond involving the phosphine-substituted ruthenium atom, consistent with other similar clusters including the Ru/S cluster $[Ru_3(\mu_3\text{-}S)_2(CO)_8(PPh_2C_2{}^tBu)]$ (2.8275(5), 2.7316(5) Å) [18]. The six Ru-S bond lengths range from 2.3711(7) to 2.4199(7) Å, the two longest Ru-S bonds involving Ru(3), the apical atom in the square pyramidal cluster core, consistent with the analogous Fe/Se cluster. The Ru(1)–P bond length, 2.2988(8) Å, is significantly shorter than those found in the selenium cluster $[Ru_3(\mu_3\text{-}Se)_2(CO)_7(PPh_3)_2]$ (2.357(2), 2.363(2) Å) [15] as the chalcogen is changed to the smaller sulfur and the level of PPh_3 substitution decreased.

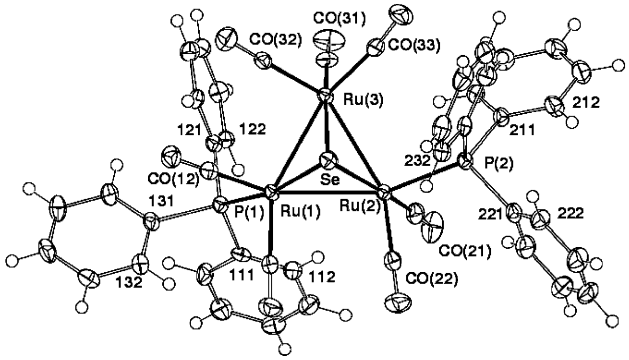

Fig. 3. Molecular projection of $[Ru_3(\mu_3\text{-}Se)(\mu_3\text{-}CO)(CO)_7(PPh_3)_2]$ (**3b**) projected down the SeH-centroid axis ($[Ru_3(\mu_3\text{-}S)(\mu_3\text{-}CO)(CO)_7(PPh_3)_2]$ (**3a**) is isostructural).

The clusters $[Ru_3(\mu_3\text{-}E)(\mu_3\text{-}CO)(CO)_7(PPh_3)_2]$ (E = S (**3a**), Se (**3b**)) (Fig. 3) are isomorphous and crystallise in the triclinic space group $P\bar{1}$ with one cluster molecule in the asymmetric unit along with one molecule of CH_2Cl_2; a contemporaneous determination of the selenide cluster **3b** has been reported at room temperature [10]. Selected crystallographic data and bond distances and angles are listed in Tables 1 and 3, respectively. The cluster core of both compounds comprises a trigonal bipyramidal $Ru_3E(CO)$ cluster geometry, where the μ_3-chalcogen and a μ_3-carbonyl ligand occupy the axial positions and three ruthenium atoms occupy the equatorial positions, forming a trigonal planar Ru_3 metal core. The two PPh_3 substituents occupy inequivalent positions, pseudo-axial and pseudo-equatorial positions, respectively, on Ru(1) and Ru(2).

The presence of the bulky PPh_3 ligands impacts significantly on the bond lengths and angles of the cluster

Table 3
Selected bond distances and angles for compounds $[Ru_3(\mu_3\text{-}E)(\mu_3\text{-}CO)(CO)_7(PPh_3)_2]$ (E = S (**3a**) (298 K), Se (**3b**) (150 K))

	S	Se		S	Se
Bond distances (Å)					
Ru(1)–Ru(2)	2.8330(10)	2.8450(6)	Ru(2)–Ru(3)	2.8506(12)	2.8654(6)
Ru(1)–Ru(3)	2.7946(13)	2.8087(6)	Ru(1)–E(1)	2.3621(13)	2.4773(5)
Ru(2)–E(1)	2.3593(9)	2.4755(7)	Ru(3)–E(1)	2.3630(10)	2.4827(7)
Ru(1)–C(11)	2.160(3)	2.153(6)	Ru(2)–C(11)	2.151(3)	2.146(5)
Ru(3)–C(11)	2.191(3)	2.184(4)	C(11)–O(11)	1.193(3)	1.198(6)
Ru(1)–P(1)	2.3655(12)	2.3536(11)	Ru(2)–P(2)	2.3585(14)	2.3565(13)
Bond angles (°)					
Ru(1)–Ru(2)–Ru(3)	58.90(3)	58.925(15)	Ru(1)–C(11)–Ru(2)	82.17(10)	82.9(2)
Ru(2)–Ru(3)–Ru(1)	60.23(3)	60.174(14)	Ru(1)–C(11)–Ru(3)	79.92(10)	80.72(18)
Ru(3)–Ru(1)–Ru(2)	60.86(3)	60.901(14)	Ru(2)–C(11)–Ru(3)	82.05(10)	82.86(15)
Ru(2)–Ru(1)–E(1)	53.08(3)	54.911(17)	Ru(2)–Ru(1)–C(11)	48.78(8)	48.45(12)
Ru(3)–Ru(1)–E(1)	53.76(3)	55.600(18)	Ru(3)–Ru(1)–C(11)	50.54(8)	50.13(11)
Ru(1)–Ru(2)–E(1)	53.17(3)	54.971(15)	Ru(1)–Ru(2)–C(11)	49.04(8)	48.66(16)
Ru(3)–Ru(2)–E(1)	52.93(2)	54.814(17)	Ru(3)–Ru(2)–C(11)	49.59(8)	49.15(11)
Ru(1)–Ru(3)–E(1)	53.72(3)	55.418(16)	Ru(1)–Ru(3)–C(11)	49.54(8)	49.15(16)
Ru(2)–Ru(3)–E(1)	52.81(3)	54.578(17)	Ru(2)–Ru(3)–C(11)	48.36(8)	47.99(12)
Ru(1)–E(1)–Ru(2)	73.75(3)	70.118(18)	P(2)–Ru(2)–Ru(1)	150.99(3)	151.10(3)
Ru(1)–E(1)–Ru(3)	72.52(4)	68.982(18)	P(2)–Ru(2)–Ru(3)	98.74(4)	99.09(3)
Ru(2)–E(1)–Ru(3)	74.26(3)	70.61(2)	P(1)–Ru(1)–E(1)	167.17(3)	167.89(4)
E(1)–Ru(1)–C(11)	87.60(8)	89.43(11)	P(1)–Ru(1)–C(11)	83.12(8)	82.86(12)
E(1)–Ru(2)–C(11)	87.87(8)	89.64(14)	P(2)–Ru(2)–E(1)	99.30(4)	97.75(4)
E(1)–Ru(3)–C(11)	86.84(8)	88.57(15)	P(2)–Ru(2)–C(11)	131.99(8)	132.53(16)
P(1)–Ru(1)–Ru(2)	123.93(3)	123.54(4)	P(1)–Ru(1)–Ru(3)	113.43(4)	112.47(4)

compounds as seen when comparing the structure of **3a** with the unsubstituted sulfide cluster, $[Ru_3(\mu_3\text{-}S)(\mu_3\text{-}CO)(CO)_9]$ [17]. The Ru–Ru bond distances of the sulfide cluster, **3a**, (2.7946(13)–2.8506(12) Å) are slightly shorter than those of the selenide analogue, **3b**, (2.8087(6)–2.8654(6) Å), as expected with the change in chalcogen, the Ru(2)-Ru(3) bond distance being longest, most probably because of steric hindrance caused by the pseudo-equatorial PPh_3 ligand. The Ru–Ru bond distances in both compounds are slightly longer than those of the unsubstituted sulfide cluster, $[Ru_3(\mu_3\text{-}S)(\mu_3\text{-}CO)(CO)_9]$ (2.786(1)–2.812(1) Å) [17]. The Ru–S bond distances in **3a** (2.3593(9)–2.3630(10) Å) are slightly longer than those in the unsubstituted sulfide cluster, $[Ru_3(\mu_3\text{-}S)(\mu_3\text{-}CO)(CO)_9]$, (2.334(2)–2.341(2) Å). The Ru-P bond distances of 2.3655(12) and 2.3585(14) Å in the sulfide cluster **3a** are comparable to those of 2.3536(11) and 2.3565(13) Å of the selenide cluster, **3b**.

The Ru–Ru–Ru bond angles are similar for both the sulfide and selenide cluster compounds, **3a** and **3b**, (S, 58.90(3)–60.86(3)°; Se, 58.925(15)–60.901(14)°). In contrast, the Ru-E-Ru bond angles vary significantly between the two clusters due to the presence of different chalcogen atoms (S, 72.52(4)–74.26(3)°; Se, 68.982(18)–70.61(2)°). In both clusters the Ru(1)–E–Ru(3) bond angle is more acute than the other two Ru-E-Ru bond angles, bearing in mind that Ru(1) and Ru(2) both have coordinated PPh_3 ligands. In contrast, the smaller Fe–Se–Fe bond angle in the iron cluster $[Fe_3(\mu_3\text{-}Se)(\mu\text{-}CO)(CO)_7(PPh_3)_2]$ is associated with the two PPh_3 coordinated iron centres where the ligands are both oriented toward the selenium atom [15].

The solid-state structure of the selenide cluster (**3b**), as previously determined at room temperature [10], is generally in agreement with the low-temperature structure determined in this study, except that, curiously, the Ru–Ru and Ru–Se bond lengths determined in this research are consistently around 0.01 Å shorter than those found in the room temperature study.

2.3. Optical-limiting properties

The optical-limiting properties of **1a,b, 2a,b, 3a, 5a,b** have been assessed using the *Z*-scan technique [19], the results from which are collected in Table 4. Closed aperture *Z*-scan is usually used to derive the nonlinear refractive index intensity coefficient n_2 by examining self-focusing or self-defocusing phenomena [20]. To determine the nonlinear absorption properties, the total transmission through a sample can be monitored by employing open-aperture *Z*-scan; we have previously discussed the utility and shortcomings of this experimental procedure to evaluate optical limiting [2], the major problem being that with nanosecond, non-time-resolved measurements the power-limiting mechanism remains obscure. A typical set of *Z*-scans (those for compound **1a**) is shown in Fig. 4.

Transmission vs. fluence plots were generated for all clusters, a representative example (that of **5a**) being shown in Fig. 5.

Table 4
Ground state and excited state cross-sections of the clusters at 523 nm

Molecule	σ_0 (10^{-18} cm^2)	σ_{eff} (10^{-18} cm^2)	λ_{max} (nm) (ε (mol^{-1} L cm^{-1}))	$\varepsilon_{523\ nm}$ (mol^{-1} L cm^{-1})
1a	2.2	66	331 (7550) 458 (6660)	574
1b	4.4	4.6	337 (6605) 467 (3972)	1000
2a	0.052	2.7	339 (5672) 474 (5107)	1300
2b	15	20	351 (9439) 488 (7362)	3951
5a	20	21	352 (10932) 505 (6173)	5299
5b	31	32	358 (11513) 522 (7260)	8195

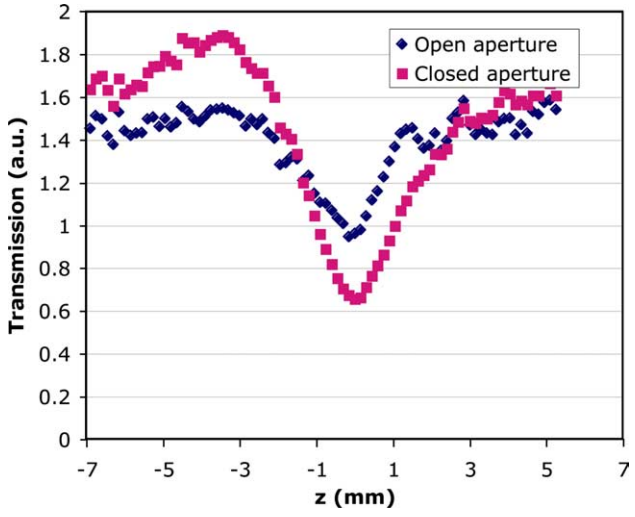

Fig. 4. Closed and open aperture Z-scans for **1a**.

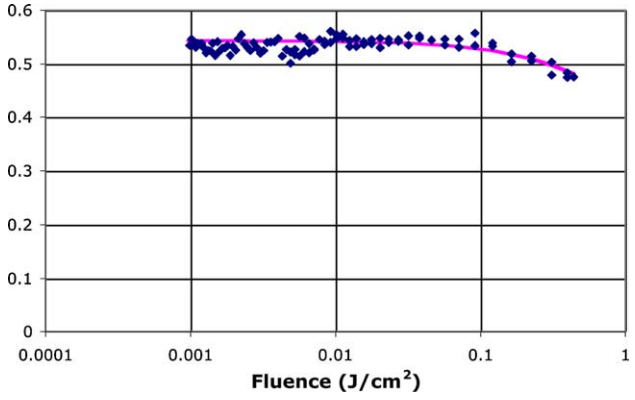

Fig. 5. Power limiting plot for **5a**.

The limiting onset in this series of compounds is at fluences on the order of 100 mJ/cm^2, some differences being seen between different samples. To quantify the power limiting properties of the different compounds we have adopted a simplified approach, treating the power limiting in the framework of formulae given in Ref. [21]. The transmittance is taken as

$$T = (1-R)^2 \frac{\exp(-\alpha_0 L)}{q} \ln(1+q),$$

where

$$q = (1-R)[1-\exp(-\alpha_0 L)]\delta_{eff} F_0 / 2F_s,$$

and R is the reflection coefficient, α_0 is the low power absorption coefficient, F_0 is the incident fluence and F_s is the saturation fluence defined as

$$F_s = \frac{\hbar\omega}{\sigma_0},$$

where σ_0 is the absorption cross section of the ground state molecules. The parameter δ_{eff} is given by

$$\delta_{eff} = \frac{\sigma_{eff} - \sigma_0}{\sigma_0},$$

where σ_{eff} is the effective absorption cross-section of the excited state molecules. The solid line in Fig. 4 has been calculated using the above equations (with $\delta_{eff} = 0.05$). The summary of the data obtained by fitting the dependences of the transmission on fluence is given in Table 4.

The effective excited-state cross-section derived by fitting the value of δ_{eff} should be treated as only a measure of the power limiting ability of the substance under given experimental conditions. The approximation used here assumes that only a single process contributes to power limiting. In practice, excited state absorption may not be the only power limiting process. The evaluation of the role of this mechanism would, however, require picosecond time-resolved experiments. With 40 ns there is a possibility that thermal contributions may also be important. Nevertheless, values of the excited-state cross-section σ_{eff} for **1a,b, 2a,b, 5a,b** are larger than those of the corresponding ground-state cross-section σ_0, i.e. all clusters are efficient optical limiters.

The optical limiting merit of a significant number of clusters have now been assessed, and by a number of different laboratories. However, the vast majority have been measured employing nanosecond pulses, which can integrate into the observed response contributions

from different mechanisms, rendering development of structure–property relationships problematical. The present series of data are consistent with **1a** being the most efficient optical limiter under our experimental conditions, but further comment is not warranted.

3. Conclusions

We have prepared the ruthenium sulfide clusters $[Ru_3(\mu_3\text{-}S)_2(CO)_8(PPh_3)]$ (**1a**), $[Ru_3(\mu_3\text{-}S)_2(CO)_7(PPh_3)_2]$ (**2a**) and $[Ru_3(\mu_3\text{-}S)(\mu_3\text{-}CO)(CO)_7(PPh_3)_2]$ (**3a**) from the reaction of $Ru_3(CO)_{12}$ with excess Ph_3PS in the presence of Me_3NO. These compounds are analogous to those prepared from the reaction of $Ru_3(CO)_{12}$ with excess Ph_3PSe [10]. Compounds **1a**, **2a** and **3a** exhibit similar $^{31}P\{^1H\}$ NMR spectra to their analogous selenide clusters and we have used DFT to show that the second species observed in the spectrum of **2a** is likely due to ligand migration from a basal ruthenium to the apical ruthenium. Single crystal X-ray diffraction studies of the monosubstituted sulfide compound, **1a**, shows the cluster core to have square pyramidal geometry consisting of a Ru_2S_2 basal plane. The structure of the monosulfide cluster, **3a**, was found to be isostructural with the selenium analogue, **3b**. The optical limiting properties of the complexes **1a,b, 2a,b, 5a,b** have been measured by the *Z*-scan technique employing 40 ns pulses at 523 nm; power limiting was observed for all clusters under our experimental conditions.

4. Experimental

4.1. General

All manipulations (prior to TLC manipulations) were carried out using standard Schlenk techniques under an atmosphere of high purity argon. Toluene and CH_2Cl_2 were dried over NaK alloy and CaH_2, respectively, under nitrogen before use. $[Ru_3(CO)_{12}]$ [22], Ph_3PE (E = S [23], Se [24]) were prepared according to literature procedures. All other reagents were obtained from Aldrich and were used without further purification. ^1H, $^{13}C\{^1H\}$ and $^{31}P\{^1H\}$ NMR spectra were recorded on a Varian Mercury Plus operating at 299.9, 75.4 and 121.4 MHz, respectively, in deuterated chloroform and referenced to the residual resonances of the solvent (δ 7.25 and 77.0, respectively) or to an external PPh_3 reference (−5.29 ppm). $Cr(acac)_3$ was added to NMR solutions prior to recording $^{13}C\{^1H\}$ NMR spectra with no pulse delay. Infrared spectra were recorded as a CH_2Cl_2 solution on a Bruker IF22 infrared spectrometer. Microanalysis (C, H, N) was determined by the Microanalytical Services, Central Science Laboratory, The University of Tasmania.

4.2. Reaction of $[Ru_3(CO)_{12}]$ with Ph_3PS

An orange solution of $[Ru_3(CO)_{12}]$ (321 mg, 0.502 mmol), Me_3NO (75 mg, 1.0 mmol) and Ph_3PS (1.180 g, 4.01 mmol) in toluene (100 mL) was stirred at 70 °C for 21 h. The reaction was monitored by TLC. The solvent was removed in vacuo to afford an orange-brown residue which was dissolved in CH_2Cl_2. Separation using preparative TLC, using CH_2Cl_2/petroleum spirits (bp 40–60 °C) (1:2) yielded four products.

1a $[Ru_3(\mu_3\text{-}S)_2(CO)_8(PPh_3)]$ (R_f 0.682, 39%) Anal. Found: C, 36.72; H, 1.67. Calc for $C_{26}H_{15}O_8PRu_3S_2$: C, 36.58; H, 1.77%. ^1H NMR (299.9 MHz, $CDCl_3$): δ 7.43–7.56 (15H, m, $P(C_6H_5)_3$). $^{13}C\{^1H\}$ NMR (75.4 MHz, $CDCl_3$): δ 203.7, 197.0, 192.8, 191.5 ($C{\equiv}O$). $^{31}P\{^1H\}$ NMR (121.4 MHz, $CDCl_3$): δ 62.65. IR (cm^{-1}): 2081(m), 2059(m), 2048(s), 2009(s), 1979(sh) (C≡Ostr).

2a $[Ru_3(\mu_3\text{-}S)_2(CO)_7(PPh_3)_2]$ (R_f 0.34, 19%) Anal. Found: C, 47.56; H, 2.77. Calc. for $C_{43}H_{30}O_7P_2Ru_3S_2$: C, 47.47; H, 2.77%. ^1H NMR (299.9 MHz, $CDCl_3$): δ 7.39–7.59 (30H, m, $P(C_6H_5)_3$). $^{13}C\{^1H\}$ NMR (75.4 MHz, $CDCl_3$): δ 203.7, 199.8, 197.6, 195.5 ($C{\equiv}O$). $^{31}P\{^1H\}$ NMR (121.4 MHz, $CDCl_3$): δ 60.2, 56.3(br), 45.5, 39.9 (br) (1:10:1:10). IR (cm^{-1}): 2054(m), 2018(s), 1979(m), 1955(m) (C≡Ostr).

3a $[Ru_3(\mu_3\text{-}S)(\mu_3\text{-}CO)(CO)_7(PPh_3)_2]$ (R_f 0.33, 14%) Anal. Found: C, 48.68; H, 2.82. Calc. for $C_{44}H_{30}O_8P_2Ru_3S$: C, 48.75; H, 2.79%. ^1H NMR (299.9 MHz, $CDCl_3$): δ 7.35–7.58 (30H, m, $P(C_6H_5)_3$). $^{13}C\{^1H\}$ NMR (75.4 MHz, $CDCl_3$): δ 207.2, 196.9 (br) ($C{\equiv}O$). $^{31}P\{^1H\}$ NMR (121.4 MHz, $CDCl_3$): δ 45.9(br), 38.8(br) (1:1). IR (cm^{-1}): 2064(m), 2024(s), 2008(s), 1971(m), 1664(w, br) (C≡Ostr).

4.3. Preparation of $[Ru_3(\mu_3\text{-}S)_2(CO)_6(PPh_3)_3]$ (**4a**)

An orange solution of $[Ru_3(\mu_3\text{-}S)_2(CO)_8(PPh_3)]$ (25 mg, 0.029 mmol), Me_3NO (4.5 mg, 0.060 mmol) and Ph_3P (30 mg, 0.11 mmol) in acetonitrile was stirred at room temperature for 16 h. TLC indicated that only $[Ru_3(\mu_3\text{-}S)_2(CO)_7(PPh_3)_2]$ had been formed. The reaction was allowed to reflux for 5 h. The reaction was monitored using TLC. The solvent was removed in vacuo to afford a dark red residue which was dissolved in CH_2Cl_2. Separation on silica, using CH_2Cl_2/petroleum spirits (bp 40–60 °C) (1:1) yielded two products identified as **2a** $[Ru_3(\mu_3\text{-}S)_2(CO)_7(PPh_3)_2]$ (trace) and **4a** $[Ru_3(\mu_3\text{-}S)_2(CO)_6(PPh_3)_3]$.

4a $[Ru_3(\mu_3\text{-}S)_2(CO)_6(PPh_3)_3]$. ($R_f$ 0.09, 89%) Anal. Found: C, 54.56; H, 3.60; S, 4.66. Calc. for $C_{60}H_{45}O_6P_3Ru_3S_2$: C, 54.50; H, 3.43; S, 4.85%. ^1H NMR (299.9 MHz, $CDCl_3$): δ 7.29–7.46 (36H, m, $P(C_6H_5)_3$), 7.62–7.69 (9H, m, $P(C_6H_5)_3$). $^{13}C\{^1H\}$ NMR (75.4 MHz, $CDCl_3$): δ 207.3, 2051, 197.1 ($C{\equiv}O$).

$^{31}P\{^1H\}$ NMR (121.4 MHz, $CDCl_3$): δ 48.20. IR (cm^{-1}): 2038(m), 2020(m), 1996(s), 1973(m), 1959(m), 1937(m), 1915(w,sh) (C≡Ostr).

4.4. Preparation of $[Ru_3(\mu_3\text{-}S)_2(CO)_7(PPh_3)_2]$

An orange solution of $[Ru_3(\mu_3\text{-}S)_2(CO)_8(PPh_3)]$ (26 mg, 0.030 mmol) and Ph_3P (10 mg, 0.038 mmol) in dichloromethane was stirred at room temperature for 26 h. The reaction was monitored by TLC. The solvent was removed in vacuo to afford an orange residue which was dissolved in CH_2Cl_2. Separation on silica, using CH_2Cl_2/petroleum spirits (bp 40–60 °C) (1:1) yielded two products identified as **2a** $[Ru_3(\mu_3\text{-}S)_2(CO)_7(PPh_3)_2]$ (90%) and **4a** $[Ru_3(\mu_3\text{-}S)_2(CO)_6(PPh_3)_3]$ (trace).

4.5. Preparation of $[Ru_3(\mu_3\text{-}Se)_2(CO)_6(PPh_3)_3]$ (*4b*)

An orange solution of $[Ru_3(\mu_3\text{-}Se)_2(CO)_7(PPh_3)_2]$ (108 mg, 0.091 mmol), Me_3NO (6.9 mg, 0.092 mmol) and Ph_3P (24 mg, 0.092 mmol) in dichloromethane was stirred at room temperature for 16 h. The reaction was monitored by TLC. The solvent was removed in vacuo to afford a dark red residue which was dissolved in CH_2Cl_2. Separation on silica, using CH_2Cl_2/petroleum spirits (bp 40–60 °C) (1:1) yielded 1 product identified as **4b** $[Ru_3(\mu_3\text{-}Se)_2(CO)_6(PPh_3)_3]$.

4b $[Ru_3(\mu_3\text{-}Se)_2(CO)_6(PPh_3)_3]$. ($R_f$ 0.08, 93%) Anal. Found: C, 50.74; H, 3.23. Calc. for $C_{60}H_{45}O_6P_3Ru_3Se_2$: C, 50.89; H, 3.20%. ^1H NMR (299.9 MHz, $CDCl_3$): δ 7.27–7.48 (36H, m, $P(C_6H_5)_3$), 7.66–7.72 (9H, m, $P(C_6H_5)_3$). $^{13}C\{^1H\}$ NMR (75.4 MHz, $CDCl_3$): δ 205.6, 196.5 (*C*≡O). $^{31}P\{^1H\}$ NMR (121.4 MHz, $CDCl_3$): δ 48.3, 46.1(br). IR (cm^{-1}): 2011(w), 1992(s), 1962(m), 1944(m,sh), 1920(w,sh) (C≡Ostr).

4.6. Reaction of $[Ru_3(\mu_3\text{-}S)(\mu_3\text{-}CO)(CO)_7(PPh_3)_2]$ with Ph_3PSe

A pale orange solution of $[Ru_3(\mu_3\text{-}S)(\mu_3\text{-}CO)(CO)_7(PPh_3)_2]$ (39 mg, 0.036 mmol), Me_3NO (2.9 mg, 0.04 mmol) and Ph_3PSe (14 mg, 0.041 mmol) in toluene (100 mL) was stirred at 70 °C for 4 h. The reaction was monitored by TLC. The solvent was removed in vacuo to afford an orange-brown residue, which was dissolved in CH_2Cl_2. Separation using preparative TLC, using CH_2Cl_2/petroleum spirits (bp 40–60 °C) (2:3) yielded two products, one identified as $[Ru_3(\mu_3\text{-}Se)_2(CO)_6(PPh_3)_3]$ (**4b**).

5 $[Ru_3(\mu_3\text{-}S)(\mu_3\text{-}Se)(CO)_7(PPh_3)_2]$ (R_f 0.15, 44%) Anal. Found: C, 45.81; H, 2.80; S, 2.96. Calc. for $C_{43}H_{30}O_7P_2Ru_3SSe$: C, 45.51; H, 2.66; S, 2.83%. ^1H NMR (299.9 MHz, $CDCl_3$):δ 7.42 –7.51 (30H, m, $P(C_6H_5)_3$). $^{13}C\{^1H\}$ NMR (75.4 MHz, $CDCl_3$): δ 207.3, 199.8, 197.1(br) (*C*≡O). $^{31}P\{^1H\}$ NMR (121.4 MHz, $CDCl_3$): δ 58.1, 55.1(br), 54.4(sh), 45.7, 44.7(br), 36.9(br). IR (cm^{-1}): 2048(s), 2013(s), 1974(m), 1950(w) (C≡Ostr).

4.7. X-ray crystallography

Orange plates of **3a** and **3b** were grown by slow evaporation of solutions of the complexes in CH_2Cl_2. Yellow prisms of **1a** were grown by slow evaporation of a solution of the complex in $CHCl_3$. Full spheres of CCD area-detector diffractometer data were measured (Bruker AXS, ω-scans, monochromatic MoK_α radiation, $\lambda = 0.7107_3$ Å), $N_{(total)}$ reflections merging to N unique (R_{int} cited) after 'empirical'/multiscan absorption correction (proprietary software), N_o with $F > 4\sigma(F)$ being considered "observed" and used in the full matrix least squares refinements. Neutral atom complex scattering factors were employed within the context of the Xtal 3.7 program system [25]. A full sphere of data for **3a** was measured (Enraf-Nonius CAD4 diffractometer), the absorption correction [26] using WinGX software [27], N_o with $I > 2\sigma(I)$ being considered "observed", computation using X-Seed [28] and Shelx97 [29] program systems. Pertinent results are given above and in the tables and figures, the latter showing 50% probability amplitude displacement ellipsoids for the non-hydrogen atoms, hydrogen atoms having arbitrary radii of 0.1 Å.

4.8. Computational methods

Full geometry optimisations were carried out with the use of the B3LYP [30–32] density functional level of theory combined with the LANL2DZ:6-31G(d) basis set (which incorporates the Hay and Wadt [33] small-core relativistic effective core potential and double-zeta valence basis set on ruthenium, together with the 6-31G(d) basis set [34–43] on all other atoms). Sets of five d-functions were used in the basis sets throughout these calculations. All calculations were carried out with the GAUSSIAN 03 [44] program on the Australian Partnership for Advanced Computing (APAC) supercomputer.

4.9. Optical limiting studies

The experiments were performed on solutions of all the compounds in dichloromethane. Linear optical spectra were obtained on a Varian Cary 5E UV–Vis–NIR Spectrophotometer over the spectral range 800–200 nm. The solutions for optical limiting studies were investigated in 1 mm glass cells. The concentrations of the compounds were adjusted in such a way as to obtain transmission of ca. 50–70% of the cell at the wavelength of the measurement. A diode-pumped Q-switched Nd:YLF laser was used for the measurements, its second-harmonic output being at the wavelength of 523 nm. The pulse duration was about 40 ns, the energy

per pulse used in the measurements was generally in the range of a few μJ/pulse and the repetition rate was set at 30 Hz. The power limiting curves were obtained by the *Z*-scan technique. Open-aperture and closed-aperture *Z*-scans were recorded simultaneously using a beam splitter. The transmission vs. *Z* data were converted into transmittance-fluence plots assuming Gaussian character of the beam with the beam Rayleigh length z_R derived by numerical fitting of the closed-aperture *Z*-scans. For most measurements in this series $z_R = 1.35$ mm.

Acknowledgments

We thank the Australian Research Council for funding of this work. We also thank Johnson-Matthey for the generous loan of $RuCl_3$. V.-A.T is an ARC Australian Postdoctoral Research Fellow and M.G.H. is an ARC Australian Professorial Fellow. We also thank the Australian Partnership for Advanced Computing (APAC) for time on the supercomputer.

Appendix A. Supplementary data

Crystallographic data for the structural analysis has been deposited with the Cambridge Crystallographic Data Centre, CCDC no. 255342–255344 for compounds **1a, 3a, 3b**. Copies of this information may be obtained free of charge from The Director, CCDC, 12 Union Road, Cambridge, CB2 1EZ, UK [fax. (int code): +44(1223)336-033] or email: deposit@ccdc.cam.ac.uk or www: http://www.ccdc.cam.ac.uk. XYZ Cartesian coordinates for all optimised structures described in this article are available as supporting information. Supplementary data associated with this article can be found, in the online version at doi:10.1016/j.jorganchem.2004.12.018.

References

[1] I.G. Dance, in: A. Williams, C. Floriani, A. Merbach (Eds.), Perspectives in Coordination Chemistry, VCH, Basel, 1992.
[2] M. Feliz, J.M. Garriga, R. Llusar, S. Uriel, M.G. Humphrey, N.T. Lucas, M. Samoc, B. Luther-Davies, Inorg. Chem. 40 (2001) 6132.
[3] S. Shi, W. Ji, J.P. Lang, X.Q. Xin, J. Phys. Chem. 98 (1994) 3570.
[4] W. Ji, S. Shi, S.H. Tang, J.P. Lang, X.Q. Xin, J. Phys. Chem. 99 (1995) 17297.
[5] Q.-F. Zhang, Y.-N. Xiong, T.-S. Lai, W. Ji, X.-Q. Xin, J. Phys. Chem. B 104 (2000) 3446.
[6] D. Cauzzim, C. Graiff, M. Lanfranchi, G. Predieri, A. Tiripicchio, J. Organomet. Chem. 536–537 (1997) 497.
[7] P. Braunstein, C. Graiff, C. Massera, G. Predieri, J. Rosé, A. Tiripicchio, Inorg. Chem. 41 (2002) 1372.
[8] D. Cauzzi, C. Graiff, M. Lanfranchi, G. Predieri, A. Tiripicchio, J. Chem. Soc., Dalton Trans. (1995) 2321.
[9] C. Graiff, G. Predieri, A. Tiripicchio, Eur. J. Inorg. Chem. (2003) 1659, and references therein.
[10] D. Belletti, D. Cauzzi, C. Graiff, A. Minarelli, R. Pattacini, G. Predieri, A. Tiripicchio, J. Chem. Soc., Dalton Trans. (2002) 3160.
[11] C.H. Wei, L.F. Dahl, Inorg. Chem. 4 (1965) 493.
[12] K. Hashizume, Y. Mizobe, M. Hidai, Organometallics 15 (1996) 3303.
[13] B.F.G. Johnson, T.M. Layer, J. Lewis, A. Martin, P.R. Raithby, J. Organomet. Chem. 429 (1992) C41.
[14] H. Brynner, J. Wachter, R. Wanninger, M. Zabel, J. Organomet. Chem. 603 (2000) 125.
[15] P. Baistrocchi, D. Cauzzo, M. Lanfranchi, G. Predieri, A. Tiripicchio, M. Tiripicchio-Camellini, Inorg. Chim. Acta 235 (1995) 173.
[16] P. Baistrocchi, M. Careri, D. Cauzzi, C. Graiff, M. Lanfranchi, P. Manini, G. Predieri, A. Tiripicchio, Inorg. Chim. Acta 252 (1996) 367.
[17] R.D. Adams, J.E. Babin, M. Tasi, Organometallics 7 (1988) 219.
[18] G. Hogarth, N.J. Taylor, A.J. Carty, A. Meyer, J. Chem. Soc., Chem. Commun. (1988) 834.
[19] M. Sheikh-bahae, A.A. Said, T. Wei, D.J. Hagan, E.W.V. Stryland, IEEE J. Quantum Electron. 26 (1990) 760–769.
[20] I.R. Whittall, A.M. McDonagh, M.G. Humphrey, M. Samoc, Adv. Organomet. Chem. 43 (1999) 349.
[21] R.L. Sutherland, Handbook of Nonlinear Optics, Marcel Dekker, New York, 1996.
[22] M.I. Bruce, C.M. Jensen, N.L. Jones, Inorg. Synth. 28 (1990) 216.
[23] H.R. Hayes, D.J. Peterson, Organic Phosphorus Compounds, Wiley–Interscience, New York, 1972, p. 341.
[24] G.M. Kosolappoff, Organophosphorus Compounds, Wiley, New York, 1950, p. 98.
[25] S.R. Hall, D.J. du Boulay, R. Olthof-Hazekamp (Eds.), The Xtal 3.7 System, University of Western Australia, Australia, 2000.
[26] A.C.T. North, D.C. Philips, F.S. Mathew, Acta Crystallogr., Sect A 24 (1968) 351.
[27] L.J. Farrugia, J. Appl. Crystallogr. 32 (1999) 837.
[28] J.J. Barbour, J. Supramol. Chem. 1 (2001) 189.
[29] G.M. Sheldrick, SHELX97, Programs for Crystal Structure Analysis, University of Göttingen, Göttingen, 1997.
[30] A.D. Becke, J. Chem. Phys. 98 (1993) 5648.
[31] P.J. Stephens, J.F. Devlin, C.F. Chabalowski, M.J. Frisch, J. Phys. Chem. 98 (1994) 11623.
[32] R.H. Hertwig, W. Koch, Chem. Phys. Lett. 268 (1997) 345.
[33] P.J. Hay, W.R. Wadt, J. Chem. Phys. 82 (1985) 299.
[34] R. Ditchfield, W.J. Hehre, J.A. Pople, J. Chem. Phys. 5 (1971) 724.
[35] W.J. Hehre, R. Ditchfield, J.A. Pople, J. Chem. Phys. 56 (1972) 2257.
[36] P.C. Hariharan, J.A. Pople, Mol. Phys. 27 (1974) 209.
[37] M.S. Gordon, Chem. Phys. Lett. 76 (1980) 163.
[38] P.C. Hariharan, J.A. Pople, Theo. Chim. Acta 28 (1973) 213.
[39] J.P. Blaudeau, M.P. McGrath, L.A. Curtiss, L. Radom, J. Chem. Phys 107 (1997) 5016.
[40] M.M. Francl, W.J. Pietro, W.J. Hehre, J.S. Binkley, D.J. DeFrees, J.A. Pople, M.S. Gordon, J. Chem. Phys. 77 (1982) 3654.
[41] R.C. Binning Jr., L.A. Curtiss, J. Comp. Chem. 11 (1990) 1206.
[42] V.A. Rassolov, J.A. Pople, M.A. Ratner, T.L. Windus, J. Chem. Phys. 109 (1998) 1223.
[43] V.A. Rassolov, M.A. Tatner, J.A. Pople, P.C. Redfern, L.A. Curtiss, J. Comp. Chem. 22 (2001) 976.
[44] M.J. Frisch, G.W. Trucks, H.B. Schlegel, G.E. Scuseria, M.A. Robb, J.R. Cheeseman, J.A. Montgomery Jr., T. Vreven, K.N. Kudin, J.C. Burant, J.M. Millam, S.S. Iyengar, J. Tomasi, V. Barone, B. Mennucci, M. Cossi, G. Scalmani, N. Rega, G.A. Petersson, H. Nakatsuji, M. Hada, M. Ehara, K. Toyota, R. Fukuda, J. Hasegawa, M. Ishida, T. Nakajima, Y. Honsa, O.

Kitao, H. Nakai, M. Klene, X. Li, J.E. Knox, H.P. Hratchian, J.B. Cross, C. Adamo, J. Jaramillo, R. Gomperts, R.E. Stratmann, O. Yazyev, A.J. Austin, R. Cammi, C. Pomelli, J.W. Ochterski, P.Y. Ayala, K. Morokuma, G.A. Voth, P. Salvador, J.J. Dannenberg, V.G. Zakrzewski, S. Dapprich, A.D. Rabuck, K. Raghavachari, J.B. Foresman, J.V. Ortiz, Q. Cui, A.G. Baboul, S. Clifford, J. Cioslowski, B.B. Stefanov, G. Liu, A. Liashenko, P. Piskorz, I. Komaromi, R.L. Martin, D.J. Fox, T. Keith, M.A. Al-Laham, C.Y. Peng, A. Nanayakkara, M. Challacombe, P.M.W. Gill, B. Johnson, W. Chen, M.W. Wong, C. Gonzalez, J.A. Pople, GAUSSIAN 03, Revision B.04, Gaussian, Inc., Pittsburgh, PA, 2003.